Mixed quantum-classical surface hopping dynamics

Steve Nielsen and Raymond Kapral[a)]
Chemical Physics Theory Group, Department of Chemistry, University of Toronto, Toronto, ON M5S 3H6, Canada

Giovanni Ciccotti
INFM and Dipartimento di Fisica, Università ''La Sapienza,'' Piazzale Aldo Moro, 2, 00185 Roma, Italy

(Received 20 December 1999; accepted 24 January 2000)

An algorithm is presented for the exact solution of the evolution of the density matrix of a mixed quantum-classical system in terms of an ensemble of surface hopping trajectories. The system comprises a quantum subsystem coupled to a classical bath whose evolution is governed by a mixed quantum-classical Liouville equation. The integral solution of the evolution equation is formulated in terms of a concatenation of classical evolution segments for the bath phase space coordinates separated by operators that change the quantum state and bath momenta. A hybrid Molecular Dynamics–Monte Carlo scheme which follows a branching tree of trajectories arising from the action of momentum derivatives is constructed to solve the integral equation. We also consider a simpler scheme where changes in the bath momenta are approximated by momentum jumps. These schemes are illustrated by considering the computation of the evolution of the density matrix for a two-level system coupled to a low dimensional classical bath. © *2000 American Institute of Physics.* [S0021-9606(00)50215-3]

I. INTRODUCTION

A knowledge of the dynamics of a quantum mechanical subsystem in contact with a many-body environment is necessary for the description of proton or electron transfer reactions, the dynamics of spin variables interacting with their surroundings, vibrational or other quantum degrees of freedom in a condensed phase system, etc. It is difficult, if not impossible, to treat condensed phase many-body systems of this type with a fully quantum theory since the Schrödinger equation cannot be solved for the large number of degrees of freedom in the subsystem and its environment.

Often the environment (also referred to as the bath) may be treated classically to a good approximation while the quantum character of the subsystem is essential for a description of its properties. This is the case when the bath is composed of massive molecules or the quantum subsystem involves spin degrees of freedom. In these circumstances one is faced with the problem of how to treat the dynamics of a mixed quantum-classical system: a quantum system coupled to a classical bath.[1,2] If the quantum dynamics takes place on a single Born–Oppenheimer surface the problem is straightforward since Newton's equations may be used to evolve the classical phase space coordinates under the Hellmann–Feynman forces corresponding to the specific quantum state of the subsystem. However, such a description does not account for the possibility that coupling to the environment may induce transitions among quantum states and these transitions may in turn influence the classical evolution: coupling to the quantum system precludes a simple description in terms of Newtonian trajectories.[3]

Different approaches have been developed to treat such systems. Our focus is on surface-hopping methods[4–6] where the dynamics of an ensemble of trajectories is followed to represent the coupled evolution of the quantum system and bath. Typically, the classical degrees of freedom evolve by Newton's equations of motion on adiabatic energy surfaces; the evolution is interrupted by ''hops'' to other adiabatic surfaces, after which classical evolution is continued on the new potential energy surface. The hopping probabilities are determined by various schemes, for example, from weights obtained from the mixing coefficients of the coherently evolving wave function of the quantum subsystem, or directly from the nonadiabatic coupling matrix elements.

The evolution equation for the density matrix of the mixed quantum-classical system used here is obtained from that for the full quantum mechanical system by carrying out a partial Wigner transformation over the environmental degrees of freedom and expanding the evolution operator in the small parameter $(m/M)^{1/2}$, where m and M are the masses of the subsystem and bath particles, respectively. The resulting mixed quantum-classical Liouville equation describes the coupled evolution of the subsystem and bath.[7] In this article we describe an algorithm that yields an exact solution for the evolution of the mixed quantum-classical density matrix in terms of surface-hopping trajectories.

In Sec. II we sketch the formal series solution of the mixed quantum-classical Liouville equation. This solution specifies all details of the interaction between the subsystem and bath. The simulation algorithm for exact surface-hopping dynamics is described in Sec. III and it is shown how the differential momentum exchanges with the bath may be computed in terms of a family of branching trajectories. A hybrid Molecular Dynamics–Monte Carlo (MD–MC) algorithm is used to obtain a solution of the integral representation of the density matrix. A simplification where the mo-

a)Electronic mail: rkapral@gatto.chem.utoronto.ca

mentum exchange with the bath takes place by momentum jumps is presented in Sec. IV and the modification of the hybrid MD–MC algorithm for this case is described. Section V considers a two-level system coupled to a low-dimensional classical bath to illustrate the implementation of the surface-hopping schemes. Features of the mixed quantum-classical dynamics are discussed in Sec. VI. The conclusions of the study are presented in Sec. VII.

II. SURFACE-HOPPING SOLUTION OF EVOLUTION EQUATION

Let the coordinate and momentum operators of the n-particle quantum subsystem be $\hat{q}$ and $\hat{p}$, respectively, and the phase space coordinates of the N-particle classical bath be (R,P). These quantities are vectors and while we shall not indicate this fact by special notation their vector character will be evident from the context in which they appear. The evolution equation for the mixed quantum classical system we use is[7,8]

$$\frac{\partial \hat{\rho}_W(R,P,t)}{\partial t} = -\frac{i}{\hbar}[\hat{H}_W,\hat{\rho}_W(t)] + \frac{1}{2}(\{\hat{H}_W,\hat{\rho}_W(t)\} - \{\hat{\rho}_W(t),\hat{H}_W\}) = -i\hat{\mathcal{L}}\hat{\rho}_W(R,P,t). \quad (1)$$

Here $\hat{\rho}_W(R,P,t)$ is the partial Wigner transform of the density matrix,

$$\hat{\rho}_W(R,P,t) = (2\pi\hbar)^{-3N}\int dz\, e^{iP\cdot z/\hbar}\left\langle R-\frac{z}{2}|\hat{\rho}(t)|R+\frac{z}{2}\right\rangle, \quad (2)$$

obtained by taking the Wigner transform[9,10] only over the bath degrees of freedom. The partial Wigner transform of the Hamiltonian is

$$\hat{H}_W(R,P) = \frac{P^2}{2M} + \hat{h}_W(R), \quad (3)$$

where $\hat{h}_W(R) = \hat{p}^2/2m + \hat{V}_W(\hat{q},R)$ with $\hat{V}_W(\hat{q},R)$ the total potential energy operator including the bath potential energy and the subsystem–bath interactions.

Typically, surface-hopping dynamics is considered with reference to adiabatic potential energy surfaces defined by the solution of the eigenvalue problem,

$$\hat{h}_W(R)|\alpha;R\rangle = E_\alpha(R)|\alpha;R\rangle, \quad (4)$$

where $\alpha \in \{\alpha^{(1)},\alpha^{(2)},\ldots,\alpha^{(l)}\}$ when there are l states in the quantum subsystem. An Eulerian view of the dynamics is considered in Eq. (1): the time independent parameters R and P label the classical phase space point under consideration and the adiabatic basis in the eigenvalue problem of Eq. (4) is defined at each point in configuration space. In this Eulerian picture the adiabatic dynamics is not considered along an evolving trajectory but we shall show how to transform to time-evolved phase space coordinates when the simulation algorithm is described. Given these considerations, it is useful to express the abstract evolution equation (1) in the adiabatic basis. Since pairs of indices enter into the representation of the density matrix in the adiabatic (or any) basis, $\rho_W^{\alpha\alpha'}(R,P,t) = \langle\alpha;R|\hat{\rho}_W(R,P,t)|\alpha';R\rangle$, it is convenient to introduce the notation $s=\alpha\alpha'$ as a collective index for the two quantum states in the density matrix element. We consistently denote the first index by a Greek letter, say α, and the second index by the same symbol with a prime, α'. Furthermore, we introduce a subscript i or j, e.g., $s_i = \alpha_i\alpha_i'$, to label different values of s. Later this index will serve to label the times at which quantum transitions occur that change the value of s_i. It is also convenient to introduce the quantities $r_{ij}^0 = \alpha_i\alpha_j$ and $r_{ij}^1 = \alpha_i'\alpha_j'$. Using this notation, in the adiabatic basis the evolution equation may be written as[7]

$$\frac{\partial \rho_W^{s_i}(R,P,t)}{\partial t} = \sum_{s_j} -i\mathcal{L}_{s_is_j}\rho_W^{s_j}(R,P,t), \quad (5)$$

where $\rho_W^{s_i}(R,P,t) = \langle\alpha_i;R|\hat{\rho}_W(R,P,t)|\alpha_i';R\rangle$, and

$$-i\mathcal{L}_{s_i,s_j} = (-i\omega_{s_i} - iL_{s_i})\delta_{r_{ij}^0}\delta_{r_{ij}^1} + J_{s_is_j}. \quad (6)$$

The adiabatic frequency difference is defined by $\omega_{s_i}(R) = (E_{\alpha_i}(R) - E_{\alpha_i'}(R))/\hbar$, while the ''classical'' Liouville operator iL_{s_i} is given by the expression

$$iL_{s_i} = \frac{P}{M}\cdot\frac{\partial}{\partial R} + \frac{1}{2}(F_W^{\alpha_i} + F_W^{\alpha_i'})\cdot\frac{\partial}{\partial P}. \quad (7)$$

Here $F_W^{\alpha_i} = -\langle\alpha_i;R|\partial\hat{V}_W(\hat{q},R)/\partial R|\alpha_i;R\rangle$ is the Hellmann–Feynman force for state α_i. If the two states α_i and α_i' are the same then evolution is by the usual classical evolution operator corresponding to the single adiabatic potential energy surface.

The second term in Eq. (6) is responsible for coupling the different adiabatic states and is given by

$$J_{s_is_j} = -\left\{\frac{P}{M}\cdot d_{ij}^0 + \frac{1}{2}\Delta E_{ij}^0\, d_{ij}^0\cdot\frac{\partial}{\partial P}\right\}\delta_{r_{ij}^1} - \left\{\frac{P}{M}\cdot d_{ij}^1 + \frac{1}{2}\Delta E_{ij}^1\, d_{ij}^1\cdot\frac{\partial}{\partial P}\right\}\delta_{r_{ij}^0}, \quad (8)$$

with the nonadiabatic coupling matrix defined as $d_{ij}^0 \equiv d_{r_{ij}^0} = \langle\alpha_i;R|\partial/\partial R|\alpha_j;R\rangle$, $d_{ij}^1 \equiv d_{r_{ij}^1}^* = \langle\alpha_i';R|\partial/\partial R|\alpha_j';R\rangle^*$, $\Delta E_{ij}^0 \equiv \Delta E_{r_{ij}^0} = E_{\alpha_i} - E_{\alpha_j}$ and $\Delta E_{ij}^1 \equiv \Delta E_{r_{ij}^1} = E_{\alpha_i'} - E_{\alpha_j'}$.

The solution of Eq. (1) in the adiabatic basis may be obtained in terms of a sequence of surface-hopping trajectories by formally integrating Eq. (5) followed by iterating the operator identity

$$e^{(A+B)t} = e^{At} + \int_0^t d\tau_1\, e^{A(t-\tau_1)}Be^{(A+B)\tau_1}, \quad (9)$$

with $A = (-i\omega_{s_i} - iL_{s_i})\delta_{r_{ij}^0}\delta_{r_{ij}^1}$ and $B = J_{s_is_j}$ to give

$$\rho_W^{s_0}(R,P,t)=e^{-(i\omega_{s_0}+iL_{s_0})t}\rho_0^{s_0}(R,P)+\sum_{s_1}\int_0^t d\tau_1\, e^{-(i\omega_{s_0}+iL_{s_0})(t-\tau_1)}J_{s_0s_1}e^{-(i\omega_{s_1}+iL_{s_1})\tau_1}\rho_0^{s_1}(R,P)$$

$$+\sum_{s_1}\sum_{s_2}\int_0^t d\tau_1\int_0^{\tau_1}d\tau_2\, e^{-(i\omega_{s_0}+iL_{s_0})(t-\tau_1)}J_{s_0s_1}e^{-(i\omega_{s_1}+iL_{s_1})(\tau_1-\tau_2)}J_{s_1s_2}e^{-(i\omega_{s_2}+iL_{s_2})\tau_2}\rho_0^{s_2}(R,P)+\cdots, \quad (10)$$

where $\rho_0^{s_i}(R,P)$ is the initial value of the density matrix. In this infinite series each subsequent term involves one additional quantum transition. In the next section we show how one may construct an algorithm to simulate this solution.

III. EXACT SURFACE-HOPPING TRAJECTORIES

The evaluation of the terms in the series solution for the density matrix requires the computation of classical trajectory segments interrupted by actions of the J operator which is responsible for quantum transitions among the adiabatic states and momentum changes in the bath resulting from these transitions.

The classical evolution is determined by the Liouville operator iL_{s_i} depending on the Hellmann–Feynman forces corresponding to the quantum adiabatic states $s_i=\alpha_i\alpha_i'$. We use the following notation for the time-reversed trajectory starting at the phase space point (R,P) at time t and evolving to time τ_1, $(\tau_1<t)$, under the mean of the Hellmann–Feynman forces for states α_i and α_i':

$$(R_{s_i,\tau_1},P_{s_i,\tau_1})=e^{-iL_{s_i}(t-\tau_1)}(R,P). \quad (11)$$

Using this notation we may use Eq. (9) to write[11]

$$e^{-(i\omega_{s_i}+iL_{s_i})(t-\tau_1)}f_{s_i}(R,P)=e^{i\int_t^{\tau_1}d\tau\,\omega_{s_i}(R_{s_i,\tau})}f_{s_i}(R_{s_i,\tau_1},P_{s_i,\tau_1})$$
$$\equiv\mathcal{W}_{s_i}(t,\tau_1)f_{s_i}(R_{s_i,\tau_1},P_{s_i,\tau_1}), \quad (12)$$

where $f_{s_i}(R,P)$ is any function. The second line of Eq. (12) defines the phase factor $\mathcal{W}$. This expression is useful in explicit computations.

The operator $J_{s_is_j}$ has two terms each comprising a multiplicative operator and an operator involving a momentum derivative. In the algorithm we consider, it is convenient to evaluate the momentum derivatives by finite differences so that

$$d_{ij}^{\kappa}\cdot\frac{\partial f(P)}{\partial P}\approx\frac{|d_{ij}^{\kappa}|}{\sigma}\left[f\left(P+\frac{\sigma}{2}\hat{d}_{ij}^{\kappa}\right)-f\left(P-\frac{\sigma}{2}\hat{d}_{ij}^{\kappa}\right)\right], \quad (13)$$

where $\kappa\in\{0,1\}$ and will be used to label the two terms in J, $\hat{d}_{ij}^{\kappa}$ is a unit vector along d_{ij}^{κ}, and σ is the finite difference step size, which should be small in relation to the scale over which f fluctuates.

Before writing a general form for the action of $J_{s_is_j}$ on any function f, it is useful to introduce a compact notation that allows us to distinguish both the two contributions of $J_{s_is_j}$ as well as the three components of each contribution (one from the multiplicative factor and two from the finite difference approximation for the momentum derivative factor). We define

$$\mathcal{A}_{ij}^{\kappa,0}(R,P)=-\frac{P}{M}\cdot d_{ij}^{\kappa},\quad \mathcal{A}_{ij}^{\kappa,\pm1}(R,P)=\mp\frac{1}{2\sigma}\Delta E_{ij}^{\kappa}|d_{ij}^{\kappa}|. \quad (14)$$

We may write $J_{s_is_j}$ as

$$J_{s_is_j}f(R,P)=\sum_{\kappa=0}^{1}\sum_{\nu=-1}^{1}\mathcal{A}_{ij}^{\kappa,\nu}(R,P)\,\delta_{r_{ij}^1,1-\kappa}f\left(R,P+\nu\frac{\sigma}{2}\hat{d}_{ij}^{\kappa}\right). \quad (15)$$

As a result of the structure of $J_{s_is_j}$, each term in the series consists of a concatenation of classical evolution segments separated by contributions coming from $\mathcal{A}_{ij}^{0,\nu}$ or $\mathcal{A}_{ij}^{1,\nu}$ terms, each of which spawns three trajectories arising from its three components labeled by ν. Thus a term with a total of n $\mathcal{A}^{0,\nu}$ or $\mathcal{A}^{1,\nu}$ factors will have 3^n trajectories contributing to its value. A schematic representation of such a branching trajectory is shown in Fig. 1.

Each term in the series solution for the density matrix involves integrations over a sequence of intermediate times τ_i. In the segment between τ_i and τ_{i+1} the system evolves under the mean Hellmann–Feynman forces corresponding to the pair of states s_i. At time $\tau_{i+1}+\epsilon$, an infinitesimal time beyond τ_{i+1}, the J operator acts and the quantum transitions which occur at this time are labeled by $r_{i+1}^0\equiv r_{i,i+1}^0=\alpha_i\alpha_{i+1}$ for $\alpha_i\to\alpha_{i+1}$ and $r_{i+1}^1\equiv r_{i,i+1}^1=\alpha_i'\alpha_{i+1}'$ for $\alpha_i'\to\alpha_{i+1}'$. Similarly, we introduce a condensed notation for the $\mathcal{A}^{\kappa,\nu}$ factors: $\mathcal{A}_{i-1,i}^{\kappa_i,\nu_i}\equiv\mathcal{A}_i^{\kappa_i,\nu_i}$.

When J acts the trajectory branches into three components as described above and our notation for trajectories [Eq. (11)] must be generalized to account for this branching process. Consider a sequence of time segments starting at time $\tau_0=t$ and labeled by the times at which J acts:

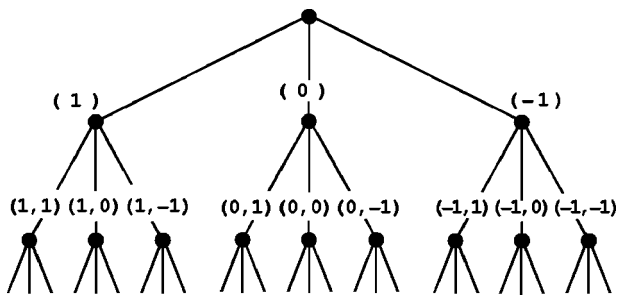

FIG. 1. Schematic representation of a branching trajectory resulting from the action of momentum derivatives that change the bath phase space points as a result of quantum transitions. The heavy dots represent J operators and the branches are labeled by $(\nu_1,\nu_2,\ldots)$.

$\{\tau_1,\tau_2,\ldots,\tau_n\}$ for a term of order n. Suppose the system starts at the phase space point (R,P) in state $s_0=\alpha_0\alpha_0'=\alpha\alpha'$ at time $\tau_0=t$, then, for evolution segments interrupted by $\mathcal{A}_{ij}^{\kappa,\nu}$ operators, the bath phase space point will evolve according to

$$
\begin{aligned}
&(R_{s_0,\tau_1},P_{s_0,\tau_1})=e^{-iL_{s_0}(t-\tau_1)}(R,P)\\
&(R_{s_1,\tau_2}^{\tau_1,\kappa_1,\nu_1},P_{s_1,\tau_2}^{\tau_1,\kappa_1,\nu_1})\\
&\quad=e^{-iL_{s_1}(\tau_1-\tau_2)}\left(R_{s_0,\tau_1},P_{s_0,\tau_1}+\nu_1\frac{\sigma}{2}\hat{d}_1^{\kappa_1}\right)\\
&\cdots\\
&(R_{s_i,\tau_{i+1}}^{\{\tau_i,\kappa_i,\nu_i\}},P_{s_i,\tau_{i+1}}^{\{\tau_i,\kappa_i,\nu_i\}})=e^{-iL_{s_i}(\tau_i-\tau_{i+1})}\\
&\left(R_{s_{i-1},\tau_i}^{\{\tau_{i-1},\kappa_{i-1},\nu_{i-1}\}},P_{s_{i-1},\tau_i}^{\{\tau_{i-1},\kappa_{i-1},\nu_{i-1}\}}+\nu_i\frac{\sigma}{2}\hat{d}_i^{\kappa_i}\right).
\end{aligned}
\tag{16}
$$

Here $\{\tau_i,\kappa_i,\nu_i\}=((\tau_1,\kappa_1,\nu_1),(\tau_2,\kappa_2,\nu_2),\ldots,(\tau_i,\kappa_i,\nu_i))$ gives the sequence of branches in the pre-history of the trajectory.

Using this notation and the results above we may write Eq. (10) as

$$
\begin{aligned}
\rho_W^{s_0}(R,P,t)=&\sum_{n=0}^{\infty}\sum_{\{s_n\}}\sum_{\{\kappa_n\}}\int_0^t d\tau_1\int_0^{\tau_1}d\tau_2\cdots\\
&\times\int_0^{\tau_{n-1}}d\tau_n X_n(\{s_n\},\{\kappa_n\},\{\tau_n\})\equiv\sum_{n=0}^{\infty}I(X_n),
\end{aligned}
\tag{17}
$$

where

$$
\begin{aligned}
&X_n(\{s_n\},\{\kappa_n\},\{\tau_n\})\\
&\quad=\sum_{\{\nu_n\}}\mathcal{W}_{s_0}(t,\tau_1)\mathcal{A}_1^{\kappa_1,\nu_1}(R_{s_0,\tau_1},P_{s_0,\tau_1})\\
&\qquad\times\mathcal{W}_{s_1}(\tau_1,\tau_2)\mathcal{A}_2^{\kappa_2,\nu_2}(R_{s_1,\tau_2}^{\tau_1,\kappa_1,\nu_1},P_{s_1,\tau_2}^{\tau_1,\kappa_1,\nu_1})\cdots\\
&\mathcal{A}_n^{\kappa_n,\nu_n}(R_{s_{n-1},\tau_n}^{\{\tau_{n-1},\kappa_{n-1},\nu_{n-1}\}},P_{s_{n-1},\tau_n}^{\{\tau_{n-1},\kappa_{n-1},\nu_{n-1}\}})\\
&\qquad\times\mathcal{W}_{s_n}(\tau_n,0)\rho_0^{s_n}(R_{s_n,0}^{\{\tau_n,\kappa_n,\nu_n\}},P_{s_n,0}^{\{\tau_n,\kappa_n,\nu_n\}}).
\end{aligned}
\tag{18}
$$

Here $\{s_n\}=(s_0,s_1,\ldots,s_n)$ with a similar notation for $\{\kappa_n\}$ and $\{\tau_n\}$. The quantity $I(X_n)$ denotes the sums and time integrals of X_n in the first equality of Eq. (17).

A. Hybrid MD–MC algorithm

We are now in a position to describe the hybrid Molecular Dynamics–Monte Carlo algorithm used to construct the exact solution for the evolution of a density matrix element. The scheme we construct allows us to compute each term of order n in the series (17) but alternate schemes may be devised for this problem where the term order is treated as a random variable and sampled by Bernoulli extractions.[12]

For a term of order n, we evaluate the summations over $\{\kappa_n\}$, $\{s_n\}$ and the n time integrals in Eq. (17) by Monte Carlo sampling using a weight function $w(\{\kappa_n\},\{s_n\},\{\tau_n\}|n)$. More specifically, the Monte Carlo estimate of a term of order n is

$$
I(X_n)=c_n\sum_{k=1}^{\mathcal{N}}X_n^{(k)}[w^{(k)}]^{-1}\equiv c_n\Phi_n,
\tag{19}
$$

where c_n is a normalization constant and k labels the realization of the stochastic process (i.e., the Monte Carlo selection of the elements of $\{s_n\}$, $\{\kappa_n\}$ and $\{\tau_n\}$) for an nth order term and $\mathcal{N}$ is the number of realizations. To compute the normalization factor we may use Monte Carlo sampling to evaluate the known integral,

$$
\begin{aligned}
&\sum_{\{s_n\}}\sum_{\{\kappa_n\}}\int_0^t\int_0^{\tau_1}\cdots\int_0^{\tau_{n-1}}d\tau_1\,d\tau_2\cdots\\
&\qquad\times d\tau_n\left(\frac{t^n}{n!}2^n(l-1)^n\right)^{-1}=1.
\end{aligned}
\tag{20}
$$

The 2^n term is due to the J branching arising from the sum over $\{\kappa_n\}$ while $(l-1)^n$ gives the number of allowed values of $\{s_n\}$. In each contribution in the off-diagonal operator J the value of α or α' is selected from the $l-1$ states to which a transition may occur. The time integrals yield the factor $t^n/n!$. The Monte Carlo evaluation of this integral gives

$$
c_n\sum_{k=1}^{\mathcal{N}}\left(\frac{t^n}{n!}2^n(l-1)^n\right)^{-1}[w^{(k)}]^{-1}\equiv c_n\Phi_n^u=1,
\tag{21}
$$

from which it follows that $c_n=1/\Phi_n^u$.

Using these results, the density matrix element may be computed by summing all orders of contributions,

$$
\rho_W^{\alpha\alpha'}(R,P,t)=\sum_{n=0}^{\infty}\frac{\Phi_n}{\Phi_n^u}.
\tag{22}
$$

In practice one tests for convergence and truncates the series at some finite value of n.

We may now give a detailed description of the algorithm and the choice of the weight function w. The algorithm must account for the random aspects mentioned above: we determine which terms in J contribute by a series of Bernoulli trials and sample the allowed values of $\{s_n\}$ and $\{\tau_n\}$ needed to evaluate the sums and integrals in Eq. (17) from suitable distributions.

The algorithm consists of the following steps if we wish to compute the quantity $\rho_W^{\alpha\alpha'}(R,P,t)$: initially we have $\tau_0=t$ and $s_0=\alpha_0\alpha_0'=\alpha\alpha'$ and bath phase space point (R,P) as given. We first compute $\mathcal{W}_{s_0}(t,0)$ and the backward evolved phase space point $(R_{s_0,0},P_{s_0,0})$. This provides the information needed to calculate a zeroth order contribution to the density matrix element [the first term in Eq. (10)]; i.e., a contribution corresponding to adiabatic dynamics with no quantum transitions. No Monte Carlo sampling or weight functions enter in the computation of this zeroth order term.

In preparation for the computation of the first order term a time $\tau_1\in[0,t]$ is chosen from a uniform distribution $p(\tau_1)=\mathcal{U}[0,t]=t^{-1}\equiv\tau_0^{-1}$ on this interval. Then we compute $\mathcal{W}_{s_0}(t,\tau_1)$ and the backward evolved phase space point $(R_{s_0,\tau_1},P_{s_0,\tau_1})$. Next, with probability $p(\alpha)$ choose α_1

$\in\{\alpha^{(1)},\alpha^{(2)},\ldots,\alpha^{(l)}\}\backslash\alpha_0$ and $\alpha_1'\in\{\alpha^{(1)},\alpha^{(2)},\ldots,\alpha^{(l)}\}\backslash\alpha_0'$ and construct $r_1^0=\alpha_0\alpha_1$ and $r_1^1=\alpha_0'\alpha_1'$. As noted earlier, we take $p(\alpha)=(l-1)^{-1}$ for simplicity in the following but other choices are possible.

First, we choose which of the two terms in J contributes to the integral. To do this we compute

$$\varphi_1=\frac{1}{\Upsilon_1}\cdot\frac{Q_1^0}{1+Q_1^0}, \tag{23}$$

where

$$\Upsilon_1=\left(\frac{Q_1^0}{1+Q_1^0}+\frac{Q_1^1}{1+Q_1^1}\right), \tag{24}$$

with

$$Q_1^\kappa=\left|\frac{P_{s_0,\tau_1}}{M}\cdot d_1^\kappa(R_{s_0,\tau_1})\right|. \tag{25}$$

We then choose either the $\kappa_1=0$ or the $\kappa_1=1$ terms in J with probabilities $p(\kappa_1=0)=\varphi_1$ and $p(\kappa_1=1)=1-\varphi_1$, respectively. If a quantum transition occurs determined by $\kappa_1=0$ then the value of $s_1=\alpha_1\alpha_0'$ while if it is determined by $\kappa_1=1$ then $s_1=\alpha_0\alpha_1'$.

We compute $\mathcal{W}_{s_1}(\tau_1,0)$, $(R_{s_1,0}^{\tau_1,\kappa_1,\nu_1},P_{s_1,0}^{\tau_1,\kappa_1,\nu_1})$ and $\mathcal{A}_1^{\kappa_1,\nu_1}(R_{s_0,\tau_1},P_{s_0,\tau_1})$ for $\nu_1=0,\pm1$. This provides the information needed to compute a contribution to the first order (a single quantum transition) term in the density matrix. In view of the above steps the weight function for the first order term is

$$w(\kappa_1,s_1,\tau_1|1)=p(\kappa_1)p(\alpha)p(\tau_1). \tag{26}$$

We now choose a time $\tau_2\in[0,\tau_1]$ from a uniform distribution with probability $p(\tau_2)=\mathcal{U}[0,\tau_1]=\tau_1^{-1}$ and compute $\mathcal{W}_{s_1}(\tau_1,\tau_2)$ and $(R_{s_1,\tau_2}^{\tau_1,\kappa_1,\nu_1},P_{s_1,\tau_2}^{\tau_1,\kappa_1,\nu_1})$ in preparation for the determination of the second order term.

The algorithm may now be continued to any order. Suppose we have chosen a time τ_n from a uniform distribution on $[0,\tau_{n-1}]$ with probability $p(\tau_n)=\mathcal{U}[0,\tau_{n-1}]=\tau_{n-1}^{-1}$. Choose α_n and α_n' with probability $p(\alpha)$ and construct $r_n^0=\alpha_{n-1}\alpha_n$ and $r_n^1=\alpha_{n-1}'\alpha_n'$. At time $\tau_n-\epsilon$, just prior to the possible action of J at time τ_n, the classical phase space coordinates of the 3^{n-1} trajectories are $(R_{s_{n-1},\tau_n}^{\{\tau_{n-1},\kappa_{n-1},\nu_{n-1}\}},P_{s_{n-1},\tau_n}^{\{\tau_{n-1},\kappa_{n-1},\nu_{n-1}\}})$. Note that all 3^{n-1} trajectories are followed and no Monte Carlo sampling is carried out on the branching tree of trajectories schematically shown in Fig. 1. As a consequence, for these higher order terms the only difference is that the choice of one of the two terms in J is made using one member of the family of 3^{n-1} trajectories as a proxy for the entire group. We choose to use the central trajectory in the branching tree, $(R_{s_{n-1},\tau_n}^{\{\tau_{n-1},\kappa_{n-1},0\}},P_{s_{n-1},\tau_n}^{\{\tau_{n-1},\kappa_{n-1},0\}})$, where $\{\tau_n,\kappa_n,0\}=((\tau_1,\kappa_1,0),(\tau_2,\kappa_2,0),\ldots,(\tau_n,\kappa_n,0))$. We then compute the quantities

$$Q_n^{\kappa_n}=\left|\frac{P_{s_{n-1},\tau_n}^{\{\kappa_{n-1},0\}}}{M}\cdot d_i^{\kappa_n}(R_{s_{n-1},\tau_n}^{\{\kappa_{n-1},0\}})\right|, \tag{27}$$

and from these construct Υ_n and φ_n in analogy to Υ_1 in Eq. (24) and φ_1 in Eq. (23), respectively. The probabilities $p(\kappa_n=0)=\varphi_n$ and $p(\kappa_n=1)=1-\varphi_n$ depend on the history of the trajectory. From the above considerations, the weight function for a term with n quantum transitions is given by

$$w(\{\kappa_n\},\{s_n\},\{\tau_n\}|n)=\prod_{i=1}^{n}p(\kappa_i)p(\alpha_i)p(\tau_i). \tag{28}$$

Note that by stopping at term order n we are in a position to calculate contributions to term orders $0,1,\ldots,n$.

Before presenting the results of calculations using this scheme it is useful to describe a modification of the algorithm when the J operators are approximated by momentum jump operators.

IV. MOMENTUM-JUMP APPROXIMATION

The operator $J_{s_is_j}$ may also be written as[7]

$$J_{s_is_j}=-\frac{P}{M}\cdot d_{ij}^0\left(1+\frac{1}{2}S_{ij}^0\cdot\frac{\partial}{\partial P}\right)\delta_{r_{ij}^1}-\frac{P}{M}\cdot d_{ij}^1\left(1+\frac{1}{2}S_{ij}^1\cdot\frac{\partial}{\partial P}\right)\delta_{r_{ij}^0}, \tag{29}$$

where S_{ij}^κ is defined as

$$S_{ij}^\kappa=\Delta E_{ij}^\kappa\, d_{ij}^\kappa\left(\frac{P}{M}\cdot d_{ij}^\kappa\right)^{-1}. \tag{30}$$

If the quantities S_{ij}^κ are sufficiently small then the operators that describe the momentum changes in the bath may be approximated by momentum translation operators,

$$(1+\tfrac{1}{2}S_{ij}^\kappa\cdot\nabla_P)\approx e^{1/2\,S_{ij}^\kappa\cdot\nabla_P}, \tag{31}$$

whose effect on any function of the momentum $f(P)$ is to change the momentum by $\frac{1}{2}S_{ij}^\kappa$:

$$e^{1/2\,S_{ij}^\kappa\cdot\partial/\partial P}f(P)=f(P+\tfrac{1}{2}S_{ij}^\kappa). \tag{32}$$

Thus, we may write

$$J_{s_is_j}\approx-\sum_{\kappa=0}^{1}\frac{P}{M}\cdot d_{ij}^\kappa e^{1/2\,S_{ij}^\kappa\cdot\nabla_P}\delta_{r_{ij}^{1-\kappa}}. \tag{33}$$

An algorithm for the calculation of the density matrix in this approximation may be constructed along the lines described above. The principal difference is that the trajectories no longer branch as a result of the action of the momentum derivatives. Instead, each time one of the components of J acts the momentum changes by $S_{ij}^\kappa/2$. Consequently, we no longer need the indices ν that label the branches but we retain the index κ to keep track of which of the two terms in J acts. Using this notation, the sequence of bath phase space coordinates at times $\tau_1,\tau_2,\ldots\tau_n$, supposing that one of the components of J acts at each of these times, is

$$(R_{s_0,\tau_1},P_{s_0,\tau_1})=e^{-iL_{s_0}(t-\tau_1)}(R,P),$$

$$(R^{\tau_1,\kappa_1}_{s_1,\tau_2},P^{\tau_1,\kappa_1}_{s_1,\tau_2})=e^{-iL_{s_1}(\tau_1-\tau_2)}\times\left(R_{s_0,\tau_1},P_{s_0,\tau_1}+\frac{S_1^{\kappa_1}}{2}\right) \tag{34}$$

$$\cdots$$

$$(R^{\{\tau_i,\kappa_i\}}_{s_i,\tau_{i+1}},P^{\{\tau_i,\kappa_i\}}_{s_i,\tau_{i+1}})=e^{-iL_{s_i}(\tau_i-\tau_{i+1})}\times\left(R^{\{\tau_{i-1},\kappa_{i-1}\}}_{s_{i-1},\tau_i},P^{\{\tau_{i-1},\kappa_{i-1}\}}_{s_{i-1},\tau_i}+\frac{S_i^{\kappa_i}}{2}\right).$$

Here $\{\tau_i,\kappa_i\}=((\tau_1,\kappa_1),(\tau_2,\kappa_2),\ldots,(\tau_i,\kappa_i))$ labels the pre-history of the choice of the two terms in J.

If we define

$$\mathcal{C}_i^{\kappa}(R,P)=-\frac{P}{M}\cdot d_i^{\kappa}, \tag{35}$$

the integrand in the nth order term in the density matrix is

$$\begin{aligned}X_n(\{s_n\},\{\kappa_n\},\{\tau_n\})=&\mathcal{W}_{s_0}(t,\tau_1)\mathcal{C}_1^{\kappa_1}(R_{s_0,\tau_1},P_{s_0,\tau_1})\\&\times\mathcal{W}_{s_1}(\tau_1,\tau_2)\\&\times\mathcal{C}_2^{\kappa_2}(R^{\tau_1,\kappa_1}_{s_1,\tau_2},P^{\tau_1,\kappa_1}_{s_1,\tau_2})\cdots\\&\times\mathcal{C}_n^{\kappa_n}(R^{\{\tau_{n-1},\kappa_{n-1}\}}_{s_{n-1},\tau_n},P^{\{\tau_{n-1},\kappa_{n-1}\}}_{s_{n-1},\tau_n})\\&\times\mathcal{W}_{s_n}(\tau_n,0)\rho_0^{s_n}(R^{\{\tau_n,\kappa_n\}}_{s_n,0},P^{\{\tau_n,\kappa_n\}}_{s_n,0}).\end{aligned} \tag{36}$$

The hybrid MD–MC algorithm closely parallels that for exact surface-hopping dynamics except that one follows a single trajectory with bath phase space coordinates given in Eq. (34). For a term with n quantum transitions the quantities Q_n^0 and Q_n^1 are defined in terms of these new phase space points as

$$Q_n^{\kappa}=\left|\frac{P^{\{\tau_{n-1},\kappa_{n-1}\}}_{s_{n-1},\tau_n}}{M}\cdot d_n^{\kappa}(R^{\{\tau_{n-1},\kappa_{n-1}\}}_{s_{n-1},\tau_n})\right|. \tag{37}$$

Note that now the Q value corresponds directly to the trajectory being propagated [see Eq. (27)]. In analogy with the previously described algorithm, we define Υ_n and φ_n in terms of the Q_n^{κ} quantities and sample the series in the same way. The density matrix elements may be estimated again by Eq. (22).

V. TWO-LEVEL SYSTEM COUPLED TO A CLASSICAL BATH

As an illustration of the above formalism we present calculations for a two-level quantum subsystem coupled to a classical bath. While we consider this case simply to demonstrate the feasibility of the technique, two-level systems of this type have been studied in many contexts and are relevant for a number of applications.[13] The partial Wigner transform of the potential energy operator $\hat{V}(\hat{q},R)$ may be written as the sum of quantum subsystem, bath and coupling terms, respectively, as $\hat{V}_W(\hat{q},R)=\hat{V}_s(\hat{q})+V_b(R)+\hat{V}_c(\hat{q},R)$. Furthermore, the Hamiltonian $\hat{h}_W(R)$ can be written in terms of the quantum subsystem Hamiltonian plus the bath and coupling potentials as $\hat{h}_W(R)=\hat{h}_s+V_b(R)+\hat{V}_c(\hat{q},R)$, with $\hat{h}_s=\hat{p}^2/2m+\hat{V}_s$. We suppose that the eigenvalue problem for $\hat{h}_s$ is

$$\hat{h}_s|i\rangle=\tilde{\epsilon}_i|i\rangle, \tag{38}$$

where the space is spanned by the two eigenstates $|1\rangle$ and $|2\rangle$. In this basis $\hat{h}_W(R)$ is

$$h_{ij}(R)=\langle i|\hat{h}_W(R)|j\rangle=(\tilde{\epsilon}_i+V_b(R))\delta_{ij}+V_{ij}(R), \tag{39}$$

where $V_{ij}(R)=\langle i|\hat{V}_c(\hat{q},R)|j\rangle$ and we further assume that $V_{ii}=0$ and $V_{12}(R)=V_{21}(R)\equiv\hbar\gamma(R)$ which couples the two subsystem states.

The solution of the eigenvalue problem for h_{ij} yields the adiabatic energies and eigenstates. The adiabatic energies are

$$E_{1,2}(R)=\overline{\epsilon}(R)\pm\frac{\hbar}{2}(\Delta^2+4\gamma(R)^2)^{1/2}, \tag{40}$$

where $\epsilon_i(R)=\tilde{\epsilon}_i+V_b(R)$, $\overline{\epsilon}(R)=(\epsilon_1(R)+\epsilon_2(R))/2$, $\Delta=(\epsilon_2(R)-\epsilon_1(R))/\hbar\equiv(\tilde{\epsilon}_2-\tilde{\epsilon}_1)/\hbar$ is the energy gap in $\hbar$ units.

The adiabatic eigenstates are

$$\begin{aligned}|1;R\rangle&=(1+G^2)^{-1/2}(|1\rangle+G|2\rangle),\\|2;R\rangle&=(1+G^2)^{-1/2}(-G|1\rangle+|2\rangle),\end{aligned} \tag{41}$$

where

$$G(R)=\frac{1}{2\gamma(R)}(-\Delta+(\Delta^2+4\gamma(R)^2)^{1/2}). \tag{42}$$

The nonadiabatic coupling matrix element is

$$d_{12}=-d_{21}=\frac{G'}{(1+G^2)}. \tag{43}$$

The contributions to the mixed quantum-classical Liouville operator in this adiabatic basis are now easily written. The Hellmann–Feynman force appearing in the classical evolution operator is

$$F_W^{1,2}=-\frac{\partial E_{1,2}(R)}{\partial R}=F_b(R)\pm2\hbar\gamma(R)\gamma'(R)\times(\Delta^2+4\gamma(R)^2)^{-1/2}, \tag{44}$$

with $\gamma'(R)=\partial\gamma(R)/\partial R$. Here F_b is the bath force, $F_b=-\partial V_b/\partial R$. The quantity S_{12} appearing in J is given by

$$S_{12}=-S_{21}=(E_1(R)-E_2(R))G'(R)\left(\frac{P}{M}\cdot G'(R)\right)^{-1}\times(\Delta^2+4\gamma(R)^2)^{1/2}G'(R)\left(\frac{P}{M}\cdot G'(R)\right)^{-1}. \tag{45}$$

These equations provide all of the ingredients needed to compute the evolution of the density matrix in terms of surface-hopping trajectories.

For the two-level system the mixed quantum-classical evolution equation takes a simple form that admits a direct numerical solution for low-dimensional baths. In the subsystem basis the evolution equation may be written as[7]

$$\frac{\partial \rho_s^{11}(R,P,t)}{\partial t} = -i\mathcal{L}^b \rho_s^{11} - 2\gamma \rho_s^{\Im} + \hbar \gamma' \cdot \frac{\partial \rho_s^{\Re}}{\partial P},$$

$$\frac{\partial \rho_s^{22}(R,P,t)}{\partial t} = -i\mathcal{L}^b \rho_s^{22} + 2\gamma \rho_s^{\Im} + \hbar \gamma' \cdot \frac{\partial \rho_s^{\Re}}{\partial P},$$

$$\frac{\partial \rho_s^{\Re}(R,P,t)}{\partial t} = -i\mathcal{L}^b \rho_s^{\Re} - \Delta \rho_s^{\Im} + \frac{\hbar \gamma'}{2} \cdot \left(\frac{\partial \rho_s^{11}}{\partial P} + \frac{\partial \rho_s^{22}}{\partial P} \right), \tag{46}$$

$$\frac{\partial \rho_s^{\Im}(R,P,t)}{\partial t} = -i\mathcal{L}^b \rho_s^{\Im} + \Delta \rho_s^{\Re} + \gamma(\rho_s^{11} - \rho_s^{22}),$$

where we have defined

$$\rho_s^{\Re} = \frac{1}{2}(\rho_s^{12} + \rho_s^{21}), \quad \rho_s^{\Im} = -\frac{i}{2}(\rho_s^{12} - \rho_s^{21}). \tag{47}$$

We have placed a subscript s on ρ to emphasize that the subsystem basis is being used. The bath Liouville operator is defined as

$$i\mathcal{L}^b = \frac{P}{M} \cdot \frac{\partial}{\partial R} + F_b(R) \cdot \frac{\partial}{\partial P}. \tag{48}$$

Once the results in the subsystem basis are obtained, the density matrix in the adiabatic basis may be found by a simple matrix multiplication to change the basis.

If the number of bath degrees of freedom is small[14] one may expand the density matrix elements in a bilinear basis of Hermite polynomials in R and P and solve the evolution equation by matrix methods. Typically, our calculations involved basis sets of approximately $N=15-20$ Hermite polynomials in each of the R and P variables and the value of N needed for convergence of the solution was tested for each computation of the density matrix. In view of the structure of Eq. (46), to obtain its solution for a one-dimensional bath matrix of size $4N^2 \times 4N^2$ must be diagonalized. These solutions constitute our standard in tests of the exact and approximate hybrid MD–MC algorithms.

VI. NUMERICAL RESULTS AND DISCUSSION

We now illustrate the above considerations with the specific example of a two-level quantum system coupled to a harmonic oscillator bath. The coupling potential is taken as $\gamma(R) = \gamma_0 R(1 + c_2 R)$, and the bath potential is taken as $V_b(R) = \frac{1}{2} M \omega_0 R^2$. We choose to work in dimensionless variables $\bar{t}$, $\bar{R}$ and $\bar{P}$ where the time is scaled by the natural bath frequency ω_0, $\bar{t} = t\omega_0$, so that $\bar{t} = 2\pi$ corresponds to one bath period, $\bar{R} = (\hbar/(M\omega_0))^{-1/2} R$ and $\bar{P} = (M\hbar\omega_0)^{-1/2} P$. In presenting results below we drop the overbar notation on dimensionless variables for simplicity and present results in dimensionless form.

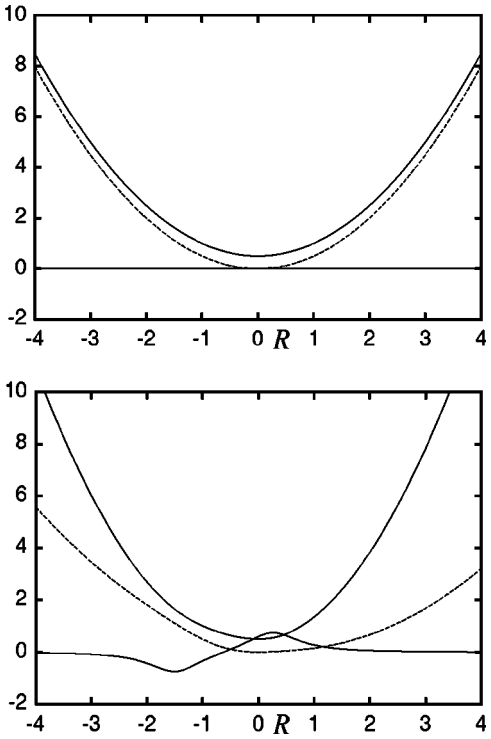

FIG. 2. Adiabatic potential energy curves $E_1(R)$ (dotted line) and $E_2(R)$ (upper solid line) are shown along with the nonadiabatic coupling matrix element $d_{12}(R)$ (lower solid line) for coupling strengths of $\gamma_0 = 0$ (upper panel) and $\gamma_0 = 0.3$, $c_2 = 0.8$ (lower panel).

The adiabatic potential energy curves arising from this model have the forms shown in Fig. 2. The c_2 parameter in the coupling potential breaks the $R=0$ reflection symmetry of the adiabatic energies.

To be concrete, we take the initial conditions as

$$\rho_s^{11}(R,P,0) = \frac{1}{2\pi} \exp[-(R^2+P^2)],$$

$$\rho_s^{22}(R,P,0) = \frac{1}{8\pi} \exp\left[-\frac{1}{4}(R^2+P^2) \right], \tag{49}$$

$$\rho_s^{\Re}(R,P,0) = \rho_s^{\Im}(R,P,0) = 0,$$

so that the two subsystem states are populated initially. Making use of the transformation in Eq. (41) we may write this initial condition in the adiabatic basis. In the adiabatic basis the initial condition contains both diagonal and off-diagonal elements. Consequently, single quantum transitions contribute to the computation of the diagonal elements of the density matrix at later times, making this type of initial condition convenient for a general discussion of the results.

In our simulations we choose to follow the ground state (diagonal) component of the density matrix at the phase space point $(R,P) = (-1,1)$ as a function of time (see Fig. 3). This point lies on the tail of the initial density distribution and provides a sensitive test of the dynamics.

Figure 3 shows three curves: the Hermite solution of the differential equation [Eq. (46)], the exact trajectory formulation [Eq. (22)] allowing for up to three quantum transitions, and its momentum-jump approximation described in Sec. IV. There are two features worth mentioning. First, the exact

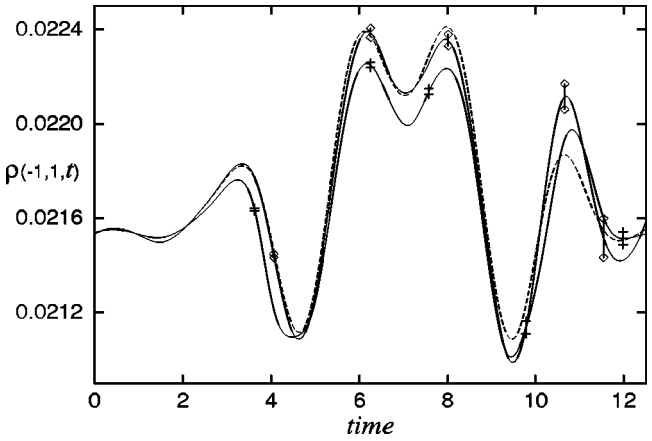

FIG. 3. The time evolution of $\rho_W^{11}(-1,1,t)$ for a coupling strength of $\gamma_0=0.05$, $c_2=0.8$. Hermite solution (broken line); momentum-jump approximation up to three jumps (lower solid curve with + error bars); exact trajectory formulation up to three jumps (upper solid curve with ◇ error bars).

trajectory result matches the Hermite solution up to $t\approx 8$. The deviations for longer times can be ascribed to the fact that the series was truncated at three quantum transitions to illustrate the effect of the neglect of higher order contributions at long times. Such higher order terms must be included to obtain accurate results at long times because the system will repeatedly access regions of nonadiabaticity. Second, the momentum-jump approximation is subject to uncontrolled errors due to the P^{-1} term in Eq. (30) which can lead to arbitrarily large momentum changes. In this example it provides a reasonable approximation to the density matrix but this is not always the case.

The contributions to the density matrix evolution are analyzed in Fig. 4 where the contributions from the zeroth order (adiabatic) and up to three quantum transition terms are presented. The system is highly nonadiabatic but the dynamics on this time scale is captured by surface-hopping trajectories involving a few quantum transitions. The different time dependent structures of the contributing nonadiabatic terms are evident from an examination of this figure.

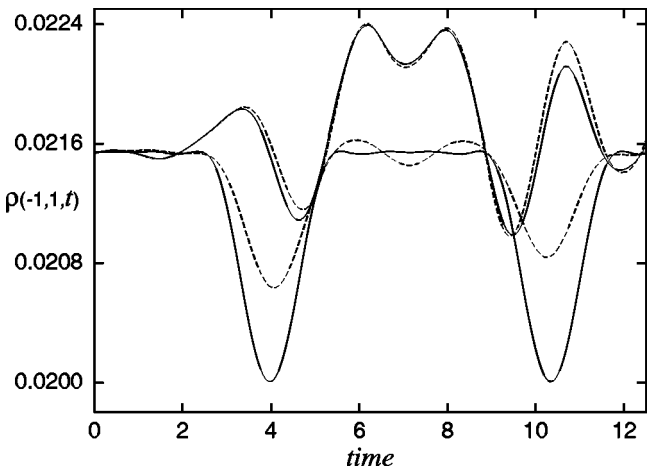

FIG. 4. The time evolution of the first four successive approximations to $\rho_W^{11}(-1,1,t)$ for a coupling strength of $\gamma_0=0.05$, $c_2=0.8$ in the exact trajectory formulation. The lower solid curve is the adiabatic result; the lower broken curve includes the first order contribution arising from one quantum transition; the upper broken curve also includes the second order contribution arising from two quantum transitions and the upper solid curve allows for up to three quantum transitions.

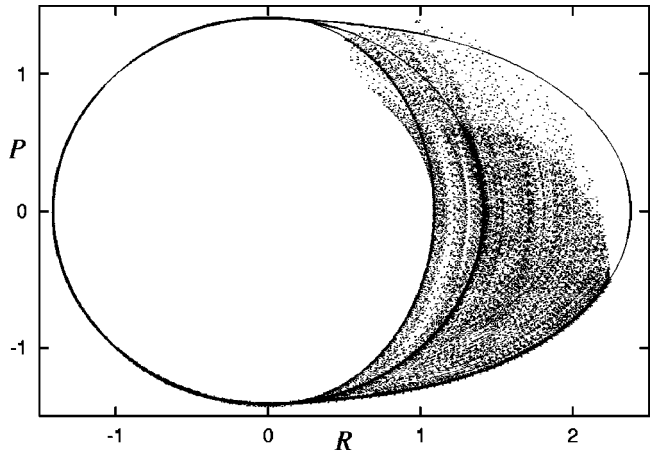

FIG. 5. The ensemble of trajectories needed to compute $\rho_W^{11}(-1,1,4.4)$ for a coupling strength of $\gamma_0=0.3$, $c_2=0.8$ in the exact trajectory formulation. The branching trajectories used to calculate momentum derivatives are not shown for clarity. The three solid closed orbits are as follows: the largest curve is obtained by propagating the phase space point $(-1,1)$ under iL_{11}, the ground state adiabatic Liouvillian. The smallest and intermediate orbits are obtained likewise under the action of iL_{22} and iL_{12}, respectively.

The trajectories underlying the exact surface-hopping algorithm provide physical insight into the nature of the nonadiabatic dynamics. This is elucidated in Figs. 5–10 and the accompanying text.

Figure 5 shows the backwards-propagating ensemble of trajectories needed to compute the quantity $\rho_W^{11}(-1,1,t)$ (shown up to $t=4.4$). Each trajectory follows either one of the two adiabatic phase space curves (governed by the Liouvillians iL_{11} and iL_{22}), or the averaged behavior[15] (governed by iL_{12}) [see Eq. (7)] and can switch between them. The

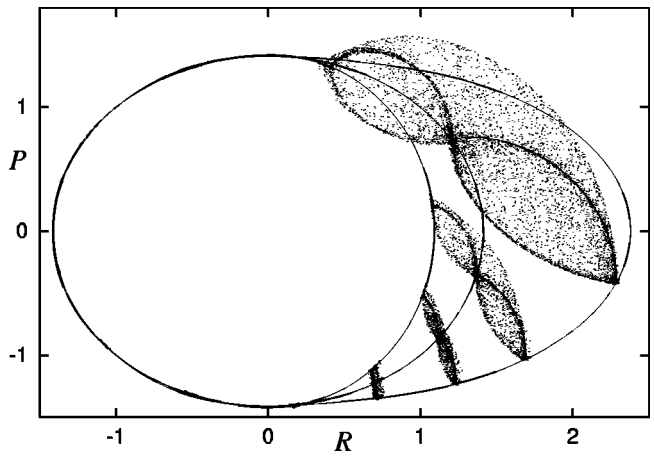

FIG. 6. The ensemble of backwards propagated phase space points needed for the evaluation of $\rho_W^{11}(-1,1,t)$ is shown for times $t=0,0.5,1.0,1.5,2.0,2.5,2.9,3.3,3.7,4.5$. Only the last four are clearly visible because the trajectories do not deviate from each other until $t\approx 2.5$. The coupling strength is $\gamma_0=0.3$, $c_2=0.8$. The branching trajectories used to calculate momentum derivatives are not shown in this and all subsequent figures for clarity.

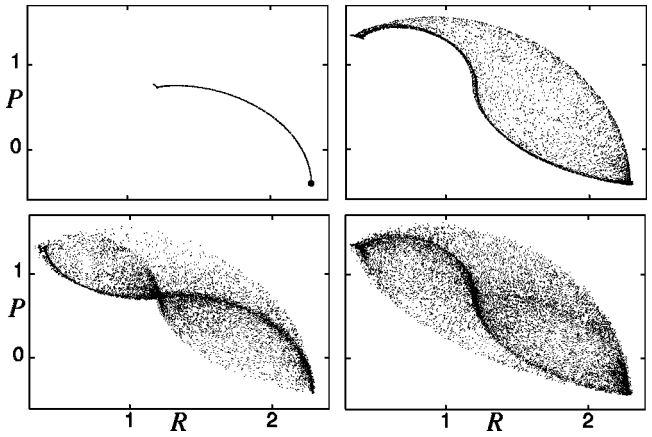

FIG. 7. The $t=4.5$ ensemble of Fig. 6 is decomposed by the number of quantum transitions allowed. The upper left panel shows the contribution from a single quantum transition, as well as the adiabatic (single point) contribution shown as an enlarged dot. The upper right, lower left, and lower right panels are the contributions from allowing exactly two, three and four quantum transitions, respectively. For clarity this four transition density has not been included in Fig. 6.

characteristic curvatures of these orbits can be seen readily in the figure. Since we are computing $\rho_W^{11}(-1,1,4.4)$, pure adiabatic evolution occurs on the outer orbit only. Each of these trajectories contributes to the integral(s) [see Eq. (10)] with a different weight. For clarity, in Fig. 5 we show only the central trajectory of the branching set of trajectories used to calculate momentum derivatives.

Plotting only the point of each trajectory corresponding to a specific propagation time t gives the results shown in Fig. 6. The bowtie-like densities are clearly tethered at each of the three adiabatic orbits which pass through the point $(R,P)=(-1,1)$. This pattern is analyzed in Fig. 7, which decomposes the longest time pattern of Fig. 6 into its constituent components. The adiabatic contribution [corresponding to the first term in Eq. (10)] evolves as a single Newtonian trajectory and is present as the enlarged lower-right point in the upper left panel of Fig. 7.

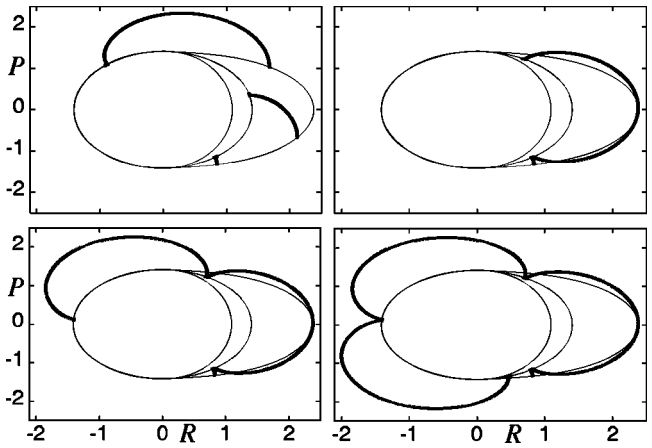

FIG. 8. Single quantum transition curves analogous to the upper left panel of Fig. 7 are shown in thick lines for $t=3.0,4.2,6.2$ (upper left panel), $t=11.3$ (upper right panel), $t=19.6$ (lower left panel) and $t=27.85$ (lower right panel). The coupling strength is $\gamma_0=0.3$, $c_2=0.8$.

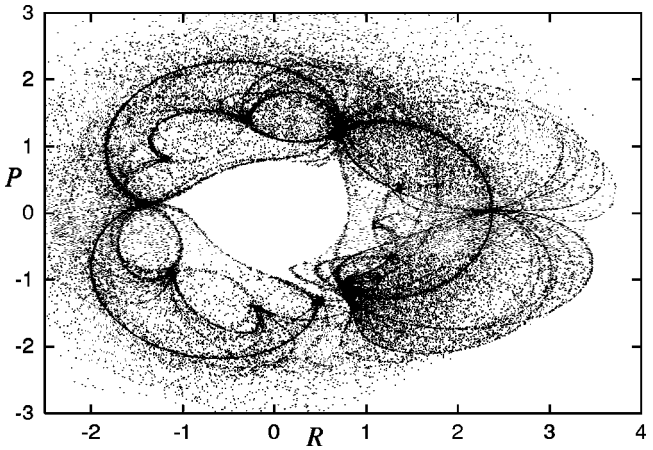

FIG. 9. The full ensemble of backwards-propagated phase space points needed for the evaluation of $\rho_W^{11}(-1,1,27.85)$ (corresponding to the lower right panel of Fig. 8). The coupling strength is $\gamma_0=0.3$, $c_2=0.8$.

This panel also contains the contribution from the second term of Eq. (10) in which a single quantum transition occurs. Since we are computing $\rho^{11}(R,P,t)$, at the point $(-1,1)$ the trajectories are all on the ground state surface under the influence of the iL_{11} Liouvillian. A single quantum transition $\alpha=1\rightarrow\alpha=2$ or $\alpha'=1\rightarrow\alpha'=2$ transfers control to the Liouvillian iL_{21} or iL_{12} [the choice arising from the two parts of J in Eq. (8)], but these are identical. The Newtonian viewpoint is not applicable in this case and instead an ensemble of trajectories must be followed to determine the density matrix element at this phase space point. Nonetheless, the resulting phase space structure is a one-dimensional curve whose lower endpoint corresponds to making a quantum transition at the last moment (or not at all), and whose upper endpoint is the result of a trajectory undergoing a quantum transition immediately following its departure from

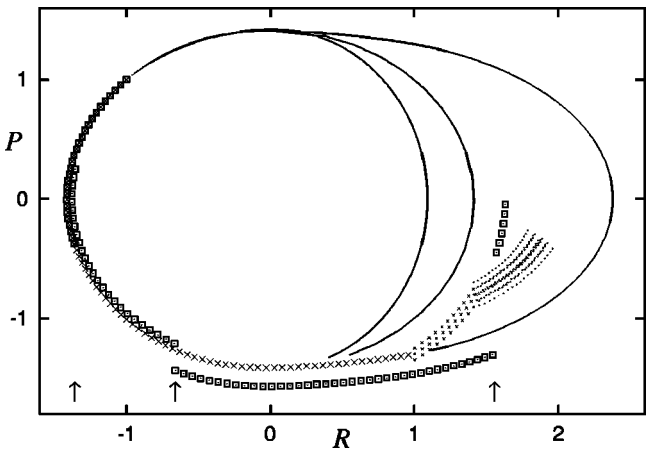

FIG. 10. A sample trajectory from each of the exact and momentum-jump algorithms for $t\approx 4$. The exact trajectory ($\times$) is continuous but is not smooth due to the effects of quantum transitions (of which there are two in this example). This trajectory lies on the adiabatic curves which have been cut away to avoid obscuring the trajectory points. The branching trajectories used to calculate momentum derivatives are shown in increasingly smaller symbols for clarity. The momentum-jump trajectory ($\square$) is subject to discontinuous momentum changes (vertical phase space jumps indicated by $\uparrow$), of which three occur in this example.

the initial point $(R,P)=(-1,1)$. The intermediate points correspond to the quantum transition occurring after staying under the iL_{11} dynamics for a time τ, and then switching to the iL_{12} dynamics for a time $t-\tau$. As τ varies from 0 to t the curve is traced out. When this switch occurs the trajectories follow the orbit induced by the iL_{12} Liouvillian which passes through the point $(R_{s_0,t-\tau},P_{s_0,t-\tau})$ [see Eq. (11)]. The family of orbits induced under this off-diagonal operator form a series of nested circles. Each point of the curve lies on a different circle of the family.

When two quantum transitions occur [corresponding to the third term of the series in Eq. (10)], the system must end up under the influence of either the iL_{11} or iL_{22} Liouvillians and, as a result, the phase space density pattern shown in the upper right panel of Fig. 7 bears no resemblance to its predecessor. When three quantum transitions occur (the lower left panel of Fig. 7), the system must end up under the influence of the iL_{12} Liouvillian but the trajectories have first visited the ground or excited adiabatic surfaces and so the resulting density pattern should resemble the one-transition plot with additional features. This is also true of the four-transition plot (shown in the lower right panel of Fig. 7) in relation to the two-transition plot, where the trajectories must end up under the influence of either the iL_{11} or iL_{22} Liouvillians.

It is instructive to follow the single quantum transition curves to much longer times, as shown in Fig. 8. In the discussion of the upper left panel of Fig. 7 we ascertained that the curve is obtained by switching to the iL_{12} dynamics after a time τ so that the trajectories follow an orbit which passes through the point $(R_{s_0,t-\tau},P_{s_0,t-\tau})$. While for Fig. 7 each point of the curve lies on a unique orbit, by $t=6.2$ (the upper left panel of Fig. 8) this is no longer the case. Some of the orbits intersect this curve twice—these same orbits twice intersect the orbit induced by iL_{11} passing through $(R,P)=(-1,1)$. These later two intersection points allow for two different times at which the dynamics can switch over to the iL_{12} Liouvillian. By $t=11.3$ (the upper right panel of Fig. 8) a second lobe has emerged. The backwards evolving trajectories now propagate long enough to pass by the $R\approx 0.2$ region twice, which is where the three adiabatic curves become distinct from one another. The second lobe emerges from trajectories that spend almost all of their time on the initial ground state surface. These observations allow for a complete understanding of single and multi-lobe curves shown in Fig. 8.

The last curve (the lower right panel of Fig. 8) is superimposed upon its higher quantum transition analogs in Fig. 9. The phase space density is highly nonuniform and has a complex structure arising from the interplay of classical evolution segments and quantum transitions described above. The structure seen in this plot can be elucidated in the same manner as was done for the single quantum transition distributions.

Finally, we show in detail what a sample trajectory looks like in both the exact trajectory and momentum-jump formulations. Once again we start the trajectories off at the phase space point $(R,P)=(-1,1)$ on the ground state adiabatic surface. We have not shown the effects of the branching nature of the exact algorithm (see Fig. 1) until now. This branching arises from the need to compute momentum derivatives, which are seeded with displaced trajectories on either side of the original one each time a quantum transition occurs. The branching of trajectories is shown in Fig. 10. There is no such branching in the momentum-jump approximation—the derivatives are replaced with momentum-jump operators. Jumps leave the R phase space variable fixed and hence are manifested as vertical discontinuities in Fig. 10.

VII. CONCLUSIONS

One of the main difficulties in constructing surface-hopping dynamics is the description of the manner in which energy is disposed in the classical degrees of freedom. The $J_{s_i s_j}$ operators in the present formulation account for bath momentum changes in a differential fashion through the momentum derivatives that appear in these operators. As described above, each time a momentum derivative acts two more trajectories are spawned so that the number of trajectories that must be followed in each realization of the dynamics increases with the term order as 3^n. If the number of quantum transitions is very large, either because the system is highly nonadiabatic or the simulation time is very long, this may be a limiting factor. However, for most applications we have in mind, for example, those relating to quantum rate processes, such simulations will be carried out in conjunction with rare event sampling which typically requires ensembles of short-time trajectories starting from unstable states. Furthermore, the methods outlined here can be embedded in schemes that utilize decoherence approximations[16] so that the description of full coherence for arbitrary times, which is implicit in the present algorithm, can be avoided. It is also possible to formulate the surface-hopping dynamics in terms of diabatic states if the system is highly nonadiabatic.

The scheme based on the momentum-jump approximation is computationally much simpler since branching trajectories due to the action of momentum derivatives are avoided. Instead, finite momentum changes are introduced in the bath when a quantum transition occurs. It should be noted that although the momentum change that is produced is proportional to that appearing in other surface-hopping schemes, the algorithm described here for its implementation is different. The momentum jumps occur in the form $S_{ij}^{\kappa}/2$ at the ends of coherent evolution segments and, thus, the way in which momentum changes in the bath and quantum transitions occur is different. For the examples and coupling strengths in this investigation the momentum-jump approximation is able to capture the main features of the density matrix evolution but its validity will depend on the system under investigation.

The numerical results presented here have served to demonstrate that exact and approximate surface-hopping methods can be successfully carried out for the evolution of the density matrix. The scheme as formulated may be directly applied to systems with classical baths comprising many degrees of freedom since one simply needs to implement standard molecular dynamics methods for the classical

evolution segments. Consequently, the hybrid MD–MC scheme for mixed quantum-classical dynamics should find application for the study of a variety of condensed phase rate problems.

ACKNOWLEDGMENT

This work was supported in part by a grant from the Natural Sciences and Engineering Research Council of Canada.

[1] J. C. Tully in *Modern Methods for Multidimensional Dynamics Computations in Chemistry*, edited by D. L. Thompson (World Scientific, New York, 1998), p. 34.
[2] M. F. Herman, Annu. Rev. Phys. Chem. **45**, 83 (1994).
[3] P. Pechukas, Phys. Rev. **181**, 166 (1969); **181**, 174 (1969).
[4] J. C. Tully, J. Chem. Phys. **93**, 1061 (1990); J. C. Tully, Int. J. Quantum Chem. **25**, 299 (1991); D. S. Sholl and J. C. Tully, J. Chem. Phys. **109**, 7702 (1998); S. Hammes-Schiffer and J. C. Tully, *ibid.* **101**, 4657 (1994).
[5] L. Xiao and D. F. Coker, J. Chem. Phys. **100**, 8646 (1994); D. F. Coker and L. Xiao, *ibid.* **102**, 496 (1995); H. S. Mei and D. F. Coker, *ibid.* **104**, 4755 (1996).
[6] F. Webster, P. J. Rossky, and R. A. Friesner, Comput. Phys. Commun. **63**, 494 (1991); F. Webster, E. T. Wang, P. J. Rossky, and R. A. Friesner, J. Chem. Phys. **100**, 4835 (1994).
[7] R. Kapral and G. Ciccotti, J. Chem. Phys. **110**, 8919 (1999).
[8] For other derivations of related equations, see W. Y. Zhang and R. Balescu, J. Plasma Phys. **40**, 199 (1988); R. Balescu and W. Y. Zhang, *ibid.* **40**, 215 (1988); C. C. Martens and J.-Y. Fang, J. Chem. Phys. **106**, 4918 (1996); A. Donoso and C. C. Martens, J. Phys. Chem. **102**, 4291 (1998).
[9] E. Wigner, Phys. Rev. **40**, 749 (1932).
[10] K. Imre, E. Özizmir, M. Rosenbaum, and P. F. Zwiefel, J. Math. Phys. **5**, 1097 (1967).
[11] Equation (12) corrects a sign error in the definition of the phase factor $\mathcal{W}$ in Eq. (41) of Ref. 7.
[12] V. S. Filinov, Yu. V. Medvedev, and V. L. Kamskyi, Mol. Phys. **85**, 711 (1995); V. S. Filinov, S. Bonella, Y. L. Lozovik, A. V. Filinov, and I. Zacharov, in *Classical and Quantum Dynamics in Condensed Phase Simulations*, edited by B. J. Berne, G. Ciccotti, and D. Coker (World Scientific, Singapore, 1998), p. 667.
[13] See, for example, A. J. Leggett, S. Chakravarty, A. T. Dorsey, M. P. A. Fisher, A. Garg, and W. Zwerger, Rev. Mod. Phys. **59**, 1 (1987); R. Silbey and R. A. Harris, J. Phys. Chem. **93**, 7062 (1989); X. Song and R. Marcus, J. Chem. Phys. **99**, 7768 (1993); M. Topaler and N. Makri, J. Phys. Chem. **100**, 4430 (1996), and references therein.
[14] Systems with low-dimensional classical baths have been used to test the validity of mixed quantum-classical schemes. See, for instance, D. Kohen, F. H. Stillinger, and J. C. Tully, J. Chem. Phys. **109**, 4713 (1998).
[15] For a two-level quantum subsystem iL_{12} is equal to the bare bath Liouvillian.
[16] E. R. Bittner and P. J. Rossky, J. Chem. Phys. **103**, 8130 (1995); O. V. Prezhdo and P. J. Rossky, Phys. Rev. Lett. **81**, 5294 (1998).